Semiclassical Calculation of Reaction Rate Constants for Homolytical Dissociation Reactions of Interest in Organometallic Vapor-Phase Epitaxy (OMVPE)

B. H. Cardelino,*,† C. E. Moore,‡ C. A. Cardelino,§ S. D. McCall,† D. O. Frazier,‡ and K. J. Bachmann#

Chemistry Department, Spelman College, Box 238, Atlanta, Georgia 30314, Space Science Laboratory, NASA George C. Marshall Space Flight Center, Huntsville, Alabama 35812, School of Earth and Atmospheric Sciences, Georgia Institute of Technology, Atlanta, Georgia 30332, and Department of Materials Science and Engineering, North Carolina State University, Raleigh, North Carolina 27695

Received: June 12, 2002; In Final Form: February 17, 2003

A procedure for calculating homolytic dissociation rate constants is reported for modeling organometallic vapor-phase epitaxy (OMVPE) of III−V compounds for all pressure regimes. Reaction rate constants were predicted following a semiclassical approach based on quantum mechanical calculations and transition-state theory. The critical configuration was determined using linear interpolations for the geometry of the intermediate structures, Morse potentials for the intermediate electronic energies, and Hase's relationship for the vibrational frequencies that become annihilated. Low-pressure rate constants were calculated from Rice−Ramsperger−Kassel−Marcus (RRKM) theory following the Troe approach. The calculations were compared with experimental values for the dissociation of one methyl radical from the closed-shell molecules $Al(CH_3)_3$, $Ga(CH_3)_3$, and $In(CH_3)_3$ and the radical molecules $Ga(CH_3)_2$ and $In(CH_3)$ and for the dissociation of one hydrogen atom from NH_3, PH_3, and AsH_3. A simplified system of reactions for the homolytic dissociation of $In(CH_3)_3$ was modeled in an OMV reactor designed for the pressure range 10^{-2} to 10^2 atm using computational fluid dynamics coupled with chemical kinetics. The steady-state simulations were carried out at 1000 K and at N_2 pressures of 1 and 20 atm.

Introduction

Organometallic vapor-phase epitaxy (OMVPE) is widely used in both scientific studies and industrial manufacturing of compound semiconductor devices and circuits. III−V compounds have been in the center of this development for many years, focusing during the past decade on group III nitrides, which permit the extension of III−V optoelectronics and photonics to the ultraviolet range of the electromagnetic spectrum.[1]

Simulations of fluid dynamics coupled to chemical reactions, transport, adsorption, and surface reactions that result in epitaxial crystal growth have been helpful in both reactor and process design. However, the set of input parameters for such computations still requires refinements, which motivates the research discussed here. In the context of a need for extending OMVPE processing to elevated pressures, new reactor designs have been recently evaluated and OMVPE systems have been built that cover the pressure range 10^{-2} to 10^2 atm. These reactors are now available for both scientific studies and process developments that can benefit from this extended capability. In this paper, we focus on predictions of unimolecular reaction kinetics regarding trimethylaluminum [$Al(CH_3)_3$], trimethylgallium [$Ga(CH_3)_3$], trimethylindium [$In(CH_3)_3$], ammonia (NH_3), phosphine (PH_3), and arsine (AsH_3) source vapor molecules and molecular fragments thereof.

A better understanding of these homolytic vapor-phase reactions is needed for high-pressure OMVPE process development. High-pressure OMVPE mandates pulsed injection of group III and group V source vapor plugs, separated by plugs of pure carrier gas. This is done to prevent homogeneous nucleation of III−V compound particles in the vapor phase. Moreover, the separate arrival of group III and V precursors to the surface of the heated substrate requires conditions of forced flow that prevent recirculation within the channel reactor. Injection of neat reactant in an inert carrier gas, under conditions precluding intermixing with reactants and products from prior pulses, leaves no other choice but a unimolecular reaction as a first step because there are simply no other reactants around. Of course, once this first step generates products, they then can enter into bimolecular reactions, unless efficient scavengers present in the vapor phase remove them. In experimental studies of the thermal decomposition of the alkyl compounds of group III elements considered here, toluene, which is known to scavenge alkyl radicals efficiently, has been used as a carrier gas.[2] We assume also the presence of scavengers, which would avoid the possibility for bimolecular reactions of fragments containing group III elements with alkyl radicals. Homogeneous bimolecular reaction kinetics resulting in adducts of fragments containing group III elements with molecules or fragments containing group V elements, which

* To whom correspondence should be addressed. E-mail: cardelino@spelman.edu. Fax: (404) 215-7874.
† Spelman College.
‡ NASA George C. Marshall Space Flight Center.
§ Georgia Institute of Technology.
# North Carolina State University.

10.1021/jp026289j CCC: $25.00
Published on Web 04/18/2003

are important intermediaries in low-pressure OMVPE, are absent under the above specified conditions. Nevertheless, pulsed-injection high-pressure OMVPE results in III−V film growth on the surface of a suitable substrate during its cyclic exposures to alternating fluxes of group III- and group V-containing precursors.

High-pressure OMVPE must be carried out at sufficiently high flow velocity to keep the Grashof number small compared to the square of the Reynolds number. At terrestrial gravity and at the upper limit of the pressure range that is presently accessible to experimentation, there is an onset of turbulence that cannot be adequately described at this time. The authors presently participate in a NASA-funded program to provide a reliable database of the effects of turbulence on the kinetics of OMVPE. They hope that their investigations will permit a comparison of the results of ground-based and space OMVPE experiments, corresponding to turbulent and laminar flow, for the same parameter set. Because the selection of optimized parameters becomes crucial when performing experiments in microgravity, the results presented in this paper are also needed for progress in the above effort. The work described in this paper builds upon previous thermochemical studies on indium compounds.[3]

We present here a method to calculate reaction rate constants for the homolytic dissociation of group III alkyl compounds and group V hydrides for modeling OMVPE. The method is based on quantum mechanical calculations and transition-state theory as described by the Rice−Ramsperger−Kassel−Marcus (RRKM) theory[4] following the Troe[5−7] approach. The results of the calculations are compared with experimental reaction rate constants for the dissociation of one methyl radical from $Al(CH_3)_3$,[8−10] $Ga(CH_3)_3$,[2,11,12] $In(CH_3)_3$,[12−14] $Ga(CH_3)_2$,[11] and $In(CH_3)$[13] and a hydrogen atom from NH_3,[15,16] PH_3,[16] and AsH_3.[16] We also present results from a simulation for the dissociation of $In(CH_3)_3$ based on a simplified model using a computational fluid dynamics program that couples heat and mass transport with chemical kinetics.

Using experimentally determined heats of formation and estimated preexponential factors, Buchan and Jasinski[16] have performed RRKM calculations on the methyl dissociation from the three organometallic compounds mentioned above and on the hydrogen radical from the three hydrides. In our work, the parameters for the initial and final states are obtained directly from quantum mechanical calculations. A classical approach is then used to determine the properties of the critical configuration required for the transition-state theory treatment. Similarly, the thermal decomposition of $Ga(CH_3)_3$ has been studied by Oikawa et al.[17] using ab initio quantum mechanical methods. In their work, they incorporate an adjustable parameter to reproduce experimental data. In our method, we do not include any adjustable parameters. Somewhat related to this study, rate constants for the decomposition of the methyl radical have been calculated by Su and Teitelbaum[18] for the falloff curves over a wide range of temperatures.

Method

According to transition-state theory,[19,20] the internal energy of a molecule may become higher than its critical energy of decomposition through collisions with other molecules. In turn, the energized molecule can become deenergized via the reverse reaction or can decompose. These three processes are characterized by the rate constants k_1, k_2, and k_3, respectively. Assuming steady state on the concentration of the energized molecule, a unimolecular rate constant, k_{uni}, for the decomposition may be defined using Lindemann's expression:[21]

$$\text{rate} = k_{uni}[\text{A}] = \frac{k_1 k_3/k_2}{1 + k_3/(k_2 P)}[\text{A}] \tag{1}$$

Equation 1 determines three pressure regimes: high, when k_{uni} is independent of pressure (denoted by k_∞); low, when k_{uni} is first-order in pressure ($k_1 P$); and the regime between the two or "falloff regime". When the definition of k_∞ is used,

$$\frac{k_{uni}}{k_\infty} = \frac{1}{1 + k_\infty/(k_1 P)} \tag{2}$$

The calculation of k_∞ for homolytic dissociation is based on the RRKM theory as applied to thermal activation.[4]

$$k_\infty = L\frac{k_B T}{h}\exp\left\{-\frac{G^{\#} - G^{UM}}{k_B T}\right\} \tag{3}$$

where L is the degeneracy of the reaction path, k_B is Boltzmann constant, T is the reaction temperature in kelvin, h is Plank constant, and $G^{\#}$ and G^{UM} are the Gibbs free energy for the activated and the unperturbed molecules, respectively. Equation 3 assumes that the translational degree of freedom along the reaction coordinate is separable from other degrees of freedom, that the transition state is located at a fixed critical reaction coordinate where the free energy of the system takes a maximum value, and that complete energy randomization is attained so that the equilibrium between the activated and the unperturbed molecule can be evaluated from the ratio between the partition functions.[22] Quack and Troe[23] discuss k_∞ in terms of a statistical adiabatic channel model. Usually the conventional transition-state theory gives the upper bound of the rate constant. An alternative approach to obtain the minimum upper limit for the position of the transition state is given by the variational statistical theory.[24,25] Wardlaw and Marcus[26,27] use a flexible transition-state approach based on RRKM theory, which accounts for the negative temperature dependence of recombination rate constants and the temperature dependence of transition-state looseness. However, flexible transition-state theory requires considerable computational effort and is currently limited to processes that involve small molecules.

At low pressures, k_1 may be obtained following the Troe[5,6] approach:

$$k_1 = \mathcal{Z}_1 \rho \frac{1}{Q_v}\exp\left\{-\frac{E_0}{k_B T}\right\} F_e F_{anh} F_{rot} F_{rot\ int} \tag{4}$$

$$\mathcal{Z}_1 = L b_c \sigma^2 \left(\frac{8\pi k_B T}{\mu}\right)^{1/2} \omega \tag{5}$$

where L is the degeneracy of the reaction path, σ is the average collision diameter, μ is the reduced mass, E_0 is the energy difference between the unperturbed and the activated molecules including zero-point energy corrections, b_c is a collision efficiency factor, ρ is the contribution to the harmonic oscillator density of states at the threshold energy, Q_v is the vibrational partition function of the activated molecule, F_e is the energy dependence of the density of states, F_{anh} is the anharmonicity of the molecular vibrations, F_{rot} is the effect of the molecular rotation, $F_{rot\ int}$ is the effect of the internal rotors, and ω is a reduced collision integral. The collision efficiency factor, b_c, is estimated from an average energy transferred per collision and

from the energy dependence of the density of states, F_e. In our calculations, the average energy transferred per collision was approximated from N_2 data. F_e is based on the number of degrees of freedom and the difference in electronic energy between the critical configuration and the unperturbed molecule, including a zero-point energy adjustment. These parameters are discussed at http://www.spelman.edu/~bcardeli. When the molecule has internal rotations, Q_v is taken as the product of a vibrational partition function and an internal rotation partition function, Q_{ir}. Using the energy barrier for each internal rotation,[3] we determine which are the harmonic vibrations that can be associated with the internal rotations. To avoid double counting, those vibrations are then eliminated from the calculation of the vibrational partition function. For the falloff region, a broadening adjustment[7] is performed on the basis of the reduced pressure and the collision efficiency factor, b_c.

Finally, the rate constant for the recombination of the products into the undissociated molecule (k_{rec}) is calculated from the value of the equilibrium constant, K_c, obtained from the Gibbs free energies of the two products of dissociation and the unperturbed molecule. It should be mentioned that, under high pressures, the recombination processes may be much more complex than assumed by this expression and may depend on the competition between capture rate, diffusion, and other reactive channels, as was determined, for example, for HCCO,[28] NO_2,[29] halogens,[30] and ethane.[31]

In summary, in the present calculations, k_∞ and k_1 are based on the determination of the partition functions for the unperturbed and activated molecules (Q^{UM} and $Q^{\#}$, respectively); in addition, k_{rec} requires also values for the partition functions of the products. The expressions used to obtain all parameters for k_∞, k_1, and k_{rec} can be obtained at http://www.spelman.edu/~bcardeli. It should be mentioned that an attempt was made to use quantum mechanics for the intermediate structures, using fixed and relaxed potential energy calculations. The converged computations alternated between different energy curves, not allowing for a smooth energy development. This is probably because the program searches for a transition state in a barrierless system and the transition state is actually not electronic but results from a maximum in the Gibbs free energy.

Determination of the Partition Function *Q*. In general, the partition function Q is assumed to be equal to the product of the following partition functions: electronic (Q_e), vibrational (Q_v), rotational (Q_r), internal rotation (Q_{ir}), and translational (Q_t). The various terms are calculated as has been previously described.[3] For the homolytic dissociation reaction, Q_e is assumed to be the same for the unperturbed molecule and the critical configuration because both structures have the same ground-state multiplicity, and at the present time, no correction is made for excited states. Q_v, the vibrational partition function, is considered to be the product of the vibrational partition functions corresponding to every vibrational mode

$$Q_v = \prod_{i=1}^{s} q_{vi}$$

In the intermediate structures, the vibrational mode that becomes imaginary along the reaction path, associated with the bond dissociation, is eliminated. Q_r, the rotational partition function, is calculated from the moments of inertia around the three coordinates. Q_{ir} is evaluated from the internal moments of inertia of all rotating groups within the molecules and their relative positions with respect to the molecular moment of inertia. The procedure distinguishes between free internal rotations and hindered rotations. To avoid double counting, the vibrational motion associated with the internal rotation is eliminated on the basis of the value of the rotational barrier.[3] At every intermediate structure, hindrance is assumed to occur if the inverse of the internal partition function ($1/q_{ir}$) is smaller than 0.95 and the rotational barrier ($u_{ir,max}$) divided by k_BT is less than 20. In the case of a hindered rotation, its contributions to the thermodynamic properties are evaluated using the tables provided by Lucas.[32] These tables have been obtained from quantum mechanical calculations. The rotational energy barrier is assumed to be the same throughout the reaction path, even though it decreases with separation as the methyl groups become farther apart. This approximation is based on the fact that the critical configuration is geometrically closer to the unperturbed molecule than to the dissociated parts and that the effect of internal rotations in heat capacity calculations for $In(CH_3)_3$ was calculated to be 16% at 100 K, dropping to 6% at 1000 K[3]. Thus, the effect of hindrance in the Gibbs free energy at higher temperatures is very small.

The calculations allow for a correction for real-gas effects by assuming that the equation of state can be approximated by $PV = zRT$, where z is the compressibility factor, and that z can be obtained from a virial correction. The equations utilized for this correction can be accessed at http://www.spelman.edu/~bcardeli.

Selection of the Critical Configuration. The critical configuration corresponds to the maximum point of the Gibbs free energy change ($G^{\#} - G^{UM}$) along the reaction path. The terms for the Gibbs free energy calculations are obtained from statistical thermodynamic calculations on the unperturbed molecule and dissociated products and on intermediate structures between the previous two structures using classically derived electronic energies and vibrational frequencies. The method consists of the following steps: (1) Quantum mechanical calculations are performed on the unperturbed molecule (UM) and on the two separating parts (MA for the major portion, MI for the minor portion) to obtain their 0 K electronic energies, E^{UM}, E^{MA} and E^{MI}, respectively, with no zero-point corrections, and their structures. R_0^{UM} corresponds to the distance between the two atoms of which the bond will break. These calculations are performed using hybrid functionals (B3LYP−UB3LYP[33,34]) within the density functional theory.[35−37] The basis sets used were 6-311G(d,p) on all atoms except In and As; for these last two atoms, 3-21g(d,p) sets were used, augmented with the AKR4 set as implemented in the Gaussian 98 quantum mechanical computer program.[38] The resulting number of basis functions has been described elsewhere.[3] (2) Quantum mechanical calculations are also performed on the UM, MA, and MI to obtain their harmonic vibrational frequencies (ν_i^{UM}, ν_i^{MA}, ν_i^{MI}) and their zero-point energy corrections as half the sum of the product of h and ν_i. (3) Q^{UM} is calculated as the product of Q_e^{UM}, Q_t^{UM}, Q_r^{UM}, Q_{ir}^{UM}, and Q_v^{UM}. (4) The UM harmonic vibrational frequencies obtained from the quantum mechanical calculations are classified into five categories, (a) those that are associated with the internal rotations of the molecule, which are excluded because they are treated as internal rotations, (b) those that have a correspondence with the vibrational frequencies of MA, (c) those that can be correlated with the vibrational frequencies of MI, (d) those frequencies that become annihilated, and (e) the vibrational frequency that leads to bond breaking (ν_0^{UM}). (5) A dissociated structure is defined with coordinates that reflect the internal parameters of the MA and MI portions. The two portions have the separating atoms along a Cartesian coordinate and are at a distance R. (6) Intermediate structures

are determined along the reaction path by linear interpolation of the Cartesian coordinates of the correlated atoms between the UM and the dissociated structure. Two hundred intermediate structures were found to be sufficient for locating the critical configuration with a precision of four significant figures. (7) The electronic energy for each intermediate structure is obtained classically by means of a Morse potential energy curve:

$$E^{\mathrm{I}} = E^{\mathrm{UM}} + E_{\mathrm{D}}\left\{1 - \exp\left[-\pi\nu_0^{\mathrm{UM}}\left(\frac{2\mu}{E_{\mathrm{D}}}\right)^{1/2}(R^{\mathrm{I}} - R_0^{\mathrm{UM}})\right]\right\}^2 \quad (6)$$

where E_{D}, the dissociation energy, is equal to $E^{\mathrm{MA}} + E^{\mathrm{MI}} - E^{\mathrm{UM}}$; μ is the reduced mass between MA and MI; and ν_0^{UM} and R_0^{UM} were previously defined. (8) All components of Q^{I} are estimated except for $Q_{\mathrm{v}}^{\mathrm{I}}$. $Q_{\mathrm{e}}^{\mathrm{I}}$ is taken to be the multiplicity of the UM. $Q_{\mathrm{t}}^{\mathrm{I}}$ is the same for all intermediate structures and equal to $Q_{\mathrm{t}}^{\mathrm{UM}}$. The rotational partition function $Q_{\mathrm{r}}^{\mathrm{I}}$ for each intermediate structure is obtained from the rotational constants along the three axes. $Q_{\mathrm{ir}}^{\mathrm{I}}$ is obtained from the moments of inertia of the rotating groups within the structure, their relative position with respect to the moments of inertia of the molecule, and their rotational barriers, as was previously described.[3] (9) The vibrational frequencies for each intermediate structure are estimated for those modes of the UM that are correlated with a mode of either MA or MI, including those that are associated with internal rotations. These vibrational frequencies are estimated, as a function of R, by linearly interpolating the two correlated frequencies. Note that the resulting value of the vibrational frequency will depend on the chosen value of R but these terms have very little effect on the overall value of the vibrational partition function $Q_{\mathrm{v}}^{\mathrm{I}}$ of the intermediate structure. (10) The vibrational frequencies for each intermediate structure are estimated for those modes of the UM that become annihilated, including those that are associated with internal rotations, using an expression derived by Hase for the decomposition of ethane:[39]

$$\nu_i^{\mathrm{I}} = \nu_i^{\mathrm{UM}} \exp\left\{-\pi\nu_0^{\mathrm{UM}}\left(\frac{2\mu}{E_{\mathrm{D}}}\right)^{1/2}(R^{\mathrm{I}} - R_0^{\mathrm{UM}})\right\} \quad (7)$$

(11) The vibrational partition functions ($Q_{\mathrm{v}}^{\mathrm{I}}$) are estimated for each intermediate structure, as well as their zero-point energy corrections ($\mathrm{ZPE}^{\mathrm{I}}$). The former is the product of the individual vibrational partition functions for every mode but eliminating those vibrations associated with the internal rotations to avoid double counting. The latter is obtained as half the sum of the product of h, the speed of light, and all ν_i^{I}, including those associated with internal rotations. It should be mentioned that the value of the partition function corresponding to a given vibration mode increases with decreasing frequency because $q_{\mathrm{v}} = (1 - e^{h\nu/(k_{\mathrm{B}}T)})^{-1}$. Consequently, $Q_{\mathrm{v}}^{\mathrm{I}}$ increases as some vibrational modes become annihilated. This is the main contribution to the increase of entropy of the system along the reaction path. The Gibbs free energy (ΔG) initially increases because of the enthalpy term (ΔH), then goes through a maximum that corresponds to the critical configuration, and then decreases because of the increase of the entropy term ($T\Delta S$) because $\Delta G \equiv \Delta H - T\Delta S$. From a quantum mechanical point of view, the Gibbs free energy should not be lower than the sum of the Gibbs free energies of the dissociation products. Thus, it is always checked that the critical configuration occurs at a distance shorter than the distance for which the Gibbs free energy reaches the value for the dissociation products. (12) The Gibbs free energy for each intermediate structure is estimated from

$$G^{\mathrm{I}} = E^{\mathrm{I}} + \mathrm{ZPE}^{\mathrm{I}} - k_{\mathrm{B}}T \ln Q^{\mathrm{I}} \quad (8)$$

The maximum value of the Gibbs free energy along the reaction path corresponds to the critical configuration and is taken as the activated molecule. Thus, the values of $G^{\#}$ and $R^{\#}$ are obtained.

Simulation of the Dissociation of Trimethylindium. Numerical simulations of the dissociation of $In(CH_3)_3$ in an OMVPE reactor were performed using the general purpose computational fluid dynamics code, CFD-ACE.[40] The physical characteristics of the model were based on an existent compact hard-shell reactor. CFD-ACE can simulate multispecies transport, heat and mass transfer (including thermal radiation), and fully coupled gas phase and surface chemistry for conventional chemical vapor deposition reactors. The simple system of reactions chosen to simulate the dissociation of trimethylindium was the following:

$$In(CH_3)_3 \leftrightarrow In(CH_3)_2 + CH_3 \quad (9)$$

$$In(CH_3)_2 \leftrightarrow In(CH_3)\text{singlet} + CH_3 \quad (10)$$

$$In(CH_3)_2 \leftrightarrow In(CH_3)\text{triplet} + CH_3 \quad (11)$$

$$In(CH_3)\text{singlet} \leftrightarrow In + CH_3 \quad (12)$$

$$In(CH_3)\text{triplet} \leftrightarrow In + CH_3 \quad (13)$$

$$In(CH_3)\text{singlet} \leftrightarrow In(CH_3)\text{triplet} \quad (14)$$

$$C_2H_6 \leftrightarrow CH_3 + CH_3 \quad (15)$$

All species were considered to be in the gas phase. No species with two In atoms were included (i.e., no In−In bond formation). No C−H bond breaking was assumed to occur because that bond breaking requires more energy than an In−C dissociation (about 300 and 200 kJ mol^{-1}, respectively). The only species with more than one multiplicity considered was $InCH_3$, which may be a singlet or a triplet with a difference in energy of 190 kJ mol^{-1}. The modeling required three types of parameters: (a) reaction rate constants, (b) thermodynamic properties for all species (ΔH, ΔS, C_p), and (c) transport properties for all species.

The reaction rate constants were obtained at 1 and 20 atm and in 99.98% N_2 gas. Equation 14 was characterized by an equilibrium constant. The reaction rate constants at both pressures, for a temperature range between 700 and 1000 K, were fit into the Arrhenius equation:

$$k = A \exp\left(\frac{-E_{\mathrm{a}}}{RT}\right) \quad (16)$$

The simulation involved entering gases at 300 K and a substrate temperature of 1000 K. Nevertheless, the Arrhenius parameters were obtained for a temperature range between 700 and 1100 K.

The values of absolute enthalpy, entropy, and heat capacity (H, S, and C_p) were obtained for two pressures (1 and 20 atm) and a range of temperatures (300−5000 K) on the basis of

the procedure previously described[3] by fitting the following equations:

$$C_p/R = z_1 + z_2T + z_3T^2 + z_4T^3 + z_5T^4 \quad (17)$$

$$H/R = z_1T + (z_2/2)T^2 + (z_3/3)T^3 + (z_4/4)T^4 + (z_5/5)T^5 + z_6 \quad (18)$$

$$S/R = z_1 \ln T + z_2T + (z_3/2)T^2 + (z_4/3)T^3 + (z_5/4)T^4 + z_7 \quad (19)$$

The coefficients z_1-z_7 were obtained directly by fitting the quantum mechanical data. However, for the fluid dynamic simulations, the z_6 and z_7 coefficients were replaced with values based on standard heats of formation and third-law entropies, respectively, such that

$$z_6 = \frac{H_f^\circ}{R} - \sum_{n=1}^{5} z_n \frac{298.15^n}{n} \quad (20)$$

$$z_7 = \frac{S_{3-\text{law}}^\circ}{R} - z_1 \ln(298.15) - \sum_{n=2}^{5} z_n \frac{298.15^{n-1}}{n-1} \quad (21)$$

The polynomial fits for the thermodynamic parameters were obtained for the range 300−5000 K because the equations provide many degrees of freedom and the selected temperature range is common in statistical thermodynamic programs. On the other hand, because the dissociation occurs in the vicinity of the substrate, which was set at 1000 K, the kinetic parameters were obtained for a range close to the substrate temperature: 700−1100 K.

The transport properties were estimated from parameters of the 6-12 Lennard-Jones and Sutherland potentials. The Sutherland parameters were obtained from the values of the 6-12 Lennard-Jones potential at intermolecular distances r greater than 10 Å. Sutherland parameters were used to evaluate viscosity.

The model for the reactor used in our simulations is based on a compact hard-shell (CHS) reactor that was built to withstand pressures up to 100 atm. Figure 1a depicts a schematic representation of an axial cross section ($x-z$ plane) of the reactor, and Figure 1b shows an assembly of machined parts that forms half of the inner core of this reactor. Two identical inner core halves are placed on top of each other and inserted into the pressure-bearing reactor shell. The reactor thus features machined inner walls, grading in and out of the entrance and exit ports, such that the flow channel formed has constant cross section from entrance to exit. Two substrate prisms heated from the back are made part of the top and bottom channel walls. Therefore, the divergence of nutrient fluxes to these substrate crystals in the top and bottom channel walls is symmetric to the centerline. The reactor is 12 in. long and has, at the substrate location, an inner channel height and width of 1 mm and 50 mm, respectively. The simulations presented here refer strictly to homogeneous gas-phase reactions based on the assumption that the substrate surface provides no sinks for the dissociation products of the organometallic compound formed in the vapor phase, that is, that no deposition occurs at the substrate.

The reduced-order model of the dissociation of trimethylindium (eqs 9−15) describes the three-dimensional transport phenomena, as well as gas-phase reactions in the flow channel of the CHS reactor, as a function of substrate temperature, total pressure, and centerline flow velocity. The high-pressure OMVPE reactor model is based on a numerical solution of nonlinear, coupled partial differential equations, representing the conservation of momentum, energy, and total mass balances over the individual species. These modeling equations are solved using the finite volume element method based upon an integral form of the equations to be solved. The computational region is divided into volumes within which the integration is carried out. The integration of the differential equations leads to a set of algebraic equations, which are solved internally by the CFD-ACE[40] using an iterative segregated solution method in which the equation sets for each variable are solved sequentially and repeatedly until a converged solution is obtained.

The boundary conditions on the momentum equations specified no slip at the solid walls. Simple thermal boundary conditions were based on the assumption of adiabatic outer wall temperatures. All walls were set to 300 K, whereas the substrate walls were set to 1000 K. The operating conditions corresponded to a flow dominated by forced convection (where the Grashof number was much smaller than the square of Reynolds number). We assumed a parabolic inlet flow velocity of 12 standard liters per minute (slm) and a constant inlet gas temperature of 300 K. The flow and heat transfer equations were solved using kinetic theory of gases. Furthermore, diffusion coefficients of individual species are solved from the Chapman−Enskog formulas based on the Lennard-Jones parameters for the gaseous species.[41]

Results and Discussion

To validate the method, calculations of rate constants were performed for three metal−alkyl compounds [$Al(CH_3)_3$, $Ga(CH_3)_3$, $In(CH_3)_3$] and three group V hydrides [NH_3, PH_3, AsH_3]. First, the experimental rate constants for the dissociation of a methyl radical from $Ga(CH_3)_3$, $Ga(CH_3)_2$, $In(CH_3)_3$ and $In(CH_3)$, obtained for specific pairs of temperature and pressure values, were compared directly with the results of the present calculations. Second, the experimentally derived Arrhenius parameters (E_a and A of eq 16) for those same reactions, as well as for the dissociation of a methyl group from $Al(CH_3)_3$ and a hydrogen radical from NH_3, PH_3, and AsH_3, were compared with the present calculations.

The quantum mechanical calculations of all undissociated metal molecules (UM) converged to C_{3h} point group except for $In(CH_3)_3$, which resulted in C_{3v}, the same point group as the group V molecules. All major portions (MA) converged to C_{2v} except for $In(CH_3)_2$; for this radical, C_2 was found to be the lowest-energy structure. The lowest energy for $Ga(CH_3)$ and $In(CH_3)$ was obtained for a singlet multiplicity. Finally, the CH_3 radical (or the minor portion, MI) had a D_{3h} point group.

Every UM atom was corresponded to either a MA atom or a MI atom. Figure 2 shows a trimethyl−metal compound before and after separation. After separation, the leaving group became planar and the dimethyl−metal radical rotated one of the methyl groups with respect to the UM because of a change in symmetry point group. For example, in the case of $Al(CH_3)_3$, the C_{3h} structure of the UM had one hydrogen of each methyl on the plane of the heavy atoms in a conrotatory way; the C_{2v} structure of the MA had the two hydrogen atoms on the plane of the heavy atoms pointing away from each other. As shown in Figure 2, the atom-to-atom correspondence was chosen as to minimize torsions.

A final distance of $R = 14$ Å for the dissociated species was chosen for the indium molecules, $R = 10$ Å for NH_3, and $R = 12$ Å for all other molecules. The criteria for selecting R were

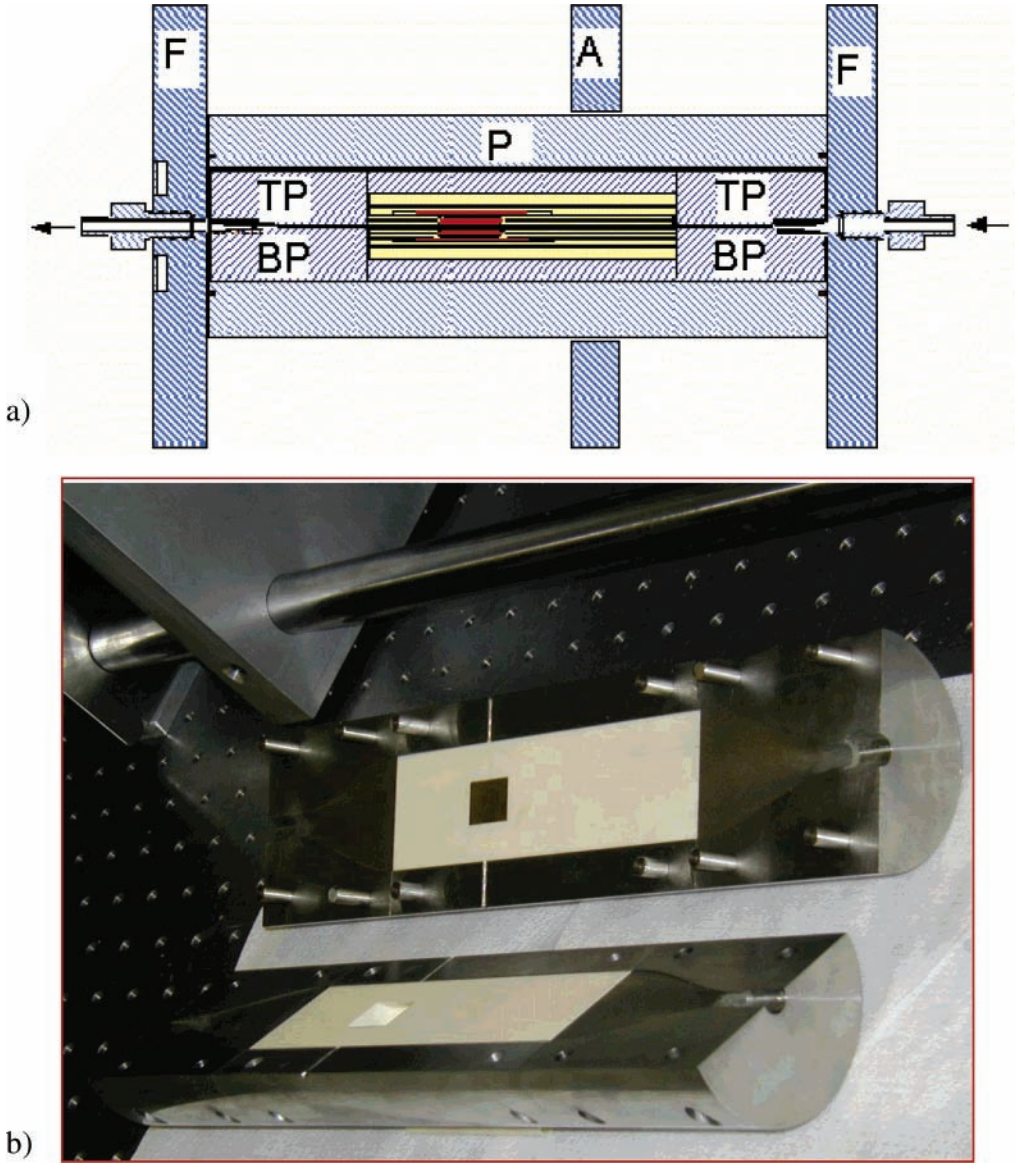

Figure 1. Schematic representation of the compact hard-shell reactor for pressure ≤ 100 atm: (a) axial cross section ($x-z$ plane), F = flange, A = adjustable flange, P = pressure-bearing vessel, TP = top plate, BP = bottom plate; (b) assembly of machined parts that form half of the inner core.

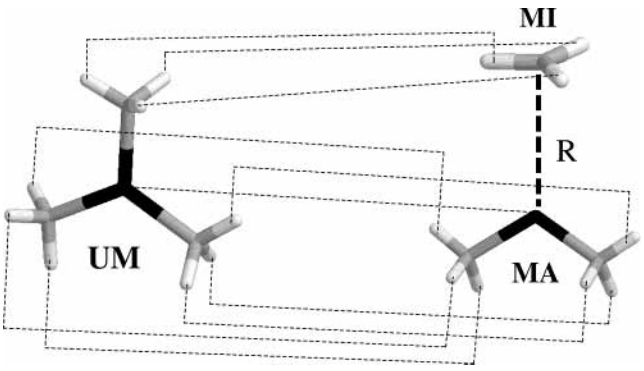

Figure 2. Unperturbed molecule (UM) of a trimethyl−metal compound and the dissociated structure with its major (MA) and minor (MI) dissociation products, the dimethyl−metal and methyl radicals, respectively. *R* corresponds to the distance between the atoms at which dissociation occurs. The figure displays the correspondence of UM atoms with the MA or MI atoms.

(a) that the electronic energy obtained from the Morse potential (eq 6) becomes equal to the sum of the electronic energy of the dissociated components to five decimal places (in au) and (b) that the vibrational frequencies, which were not correlated with either the MA or the MI portions (eq 7), become annihilated to at least three decimal places (in cm^{-1}). The values of the parameters used in eqs 6 and 7 are shown in Table 1.

The Arrhenius relationship (eq 16) indicates that the most critical parameter in the calculation of reaction rate constants is the uncertainty in the activation energy. This parameter is derived from the bond dissociation energy, which we determine using density functional theory. To evaluate the uncertainty of our calculations in this respect, we compare experimental dissociation energies for the scission of one hydrogen atom from the three hydrides. Berkowitz et al.[42] report the values of 446, 345, and 313 kJ mol^{-1} (0.170, 0.131, and 0.119 au) for NH_3, PH_3, and AsH_3, respectively. If we include zero-point energy correction to the values reported in Table 1, we obtain 0.164, 0.126, and 0.116 au, respectively. The underestimated energies for NH_3, PH_3, and AsH_3, respectively, would translate into an overestimation of the rate constants at, for example, 800 K by factors of 12, 7, and 4, respectively.

TABLE 1: Parameters for Estimating Electronic Energy as a Function of Bond Separation Based on the Morse Function $E^{I} = E^{UM} + E_D\{1 - \exp[-\pi\nu_0^{UM}(2\mu/E_D)^{1/2}(R^I - R_o^{UM}]\}^{2a}$

species	R_o^{UM} (Å)	E_D (au)	E^{UM} (au)	μ (g mol^{-1})	ν_0^{UM} (cm^{-1})
$In(CH_3)_3$	2.208	0.099	−5858.469	13.612	488
$In(CH_3)$ singlet	2.269	0.088	−5778.618	13.285	418
$In(CH_3)$ triplet to In doublet	2.345	0.016	−5778.545	13.285	301
$In(CH_3)$ triplet to In quartet		0.167			
$Ga(CH_3)_3$	1.991	0.117	−2044.651	13.044	559
$Ga(CH_3)_2$	2.022	0.052	−2004.681	12.743	655
$Al(CH_3)_3$	1.971	0.128	−362.253	11.891	640
AsH_3	1.525	0.125	−2237.674	0.995	2194
PH_3	1.424	0.138	−343.174	0.948	2391
NH_3	1.016	0.179	−56.576	0.948	3579

[a] Note that superscript I = intermediate structure, superscript UM = undissociated molecule, R_o^{UM} = equilibrium bond distance; E_D = dissociation energy; E^{UM} = equilibrium electronic energy of the undissociated molecule; μ = reduced mass between the dissociating parts; ν_0^{UM} = harmonic vibrational frequency of the dissociating bond; $R^{\#}$ = bond distance at critical configuration.

The harmonic vibrational frequencies of the UM were associated with the vibrational frequencies of the MA and MI portions, and those frequencies that were to become annihilated from the UM, as well as the one that corresponded to the bond breaking, were determined. The latter were 488, 559, and 641 cm^{-1} for $In(CH_3)_3$, $Ga(CH_3)_3$, and $Al(CH_3)_3$, respectively, 2193, 2391, and 3579 cm^{-1} for AsH_3, PH_3, and NH_3, respectively, and 418 and 512 cm^{-1} for $In(CH_3)$ and $Ga(CH_3)_2$, respectively. Symmetry and energy considerations were used to assign correspondence between the harmonic vibrational frequencies of the UM and those of the dissociating pieces MA and MI.

With respect to the partition functions, it was seen that Q_{ir} practically did not change with increasing distance between the two molecular portions and Q_r displayed a very small increase with increasing distance. Q_t was a constant value. On the other hand, Q_v was affected all along the reaction path, and by far, it was the most important term.

The distance of the critical configuration decreased with increasing temperature. At the critical configuration, the electronic energy was still rapidly increasing with distance and, in any case, it occurred way before the selected R distance for the dissociated structure.

Values of reaction rate constants at specific temperature and pressure values have been reported for a methyl dissociation from $In(CH_3)_3$, $In(CH_3)$, $Ga(CH_3)_3$, and $Ga(CH_3)_2$. Thus, to compare directly the predicted reaction rate constants with the experimental measurements, under the same conditions (pressure, temperature, carrier gas and dilution factor), average ratios have been calculated and summarized in Table 2. In addition, Arrhenius parameters have been reported for these reactions, as well as for the dissociation of a methyl group from $Al(CH_3)_3$ and a hydrogen atom from AsH_3, PH_3, and NH_3, obtained at a given pressure and for a range of temperatures. Table 3 contains the predicted and reported Arrhenius parameters for these reactions and displays the ratios between the predicted rate constant and its measured counterpart obtained from the reported Arrhenius parameters at an average temperature. The predicted values for Table 3 are also based on the same pressure, temperature range, carrier gas, and dilution factors as the experimental values. These conditions are indicated in the tables. As additional information, Table 3 also contains the predicted Arrhenius parameters for k_∞.

TABLE 2: Ratios between Calculated and Experimental Rate Constants Obtained at Specific Temperatures and Pressures[a]

	average ratio	
	without broadening	with broadening
$In(CH_3)_3 \rightarrow In(CH_3)_2 + CH_3$	1	2
$T = 550-663$ K; $P = 6.2-33.5$ Torr;		
25 points; [toluene]/[$In(CH_3)_3$] > 150 [13]		
$In(CH_3) \rightarrow In + CH_3$		
$T = 680-781$ K; $P = 6.1-33.2$ Torr;		
25 points; [toluene]/[$In(CH_3)_3$] > 150 [13]		
$In(CH_3)$ singlet to In doublet	1/181	1/92
$In(CH_3)$ triplet to In doublet	2×10^6	3×10^6
$In(CH_3)$ triplet to In quartet	$1/(6 \times 10^{14})$	$1/(3 \times 10^{14})$
$Ga(CH_3)_3 \rightarrow Ga(CH_3)_2 + CH_3$	4	8
$T = 550-663$ K; $P = 6.2-31.1$ Torr;		
37 points; [toluene]/[$Ga(CH_3)_3$] = 45−120 [11]		
$Ga(CH_3)_2 \rightarrow Ga(CH_3) + CH_3$		
$T = 829-983$ K; $P = 6.2-29.1$ Torr;		
20 points; [toluene]/[$Ga(CH_3)_3$] = 45−120 [11]		
$Ga(CH_3)$ singlet	1675	3267
$Ga(CH_3)$ triplet	1/30	1/16

[a] The broadening effect refers to a fall-off broadening correction (please refer to the section entitled Method).

Table 2 includes comparisons in which the calculations were performed with and without the broadening effect for the falloff region. Smith and Patrick[12] argued that the experimental data contained in this table was obtained at the falloff region. Inclusion of the broadening effect does not seem to improve the comparison between our calculations and the experimental values for $In(CH_3)_3$ and $Ga(CH_3)_3$ but does so for singlet In-(CH_3) and $Ga(CH_3)_2$ to triplet $Ga(CH_3)$.

As shown in Table 2, the methyl decomposition for $InCH_3$ and $Ga(CH_3)_2$ were calculated for $InCH_3$ and $Ga(CH_3)$ in singlet and triplet states. A comparison with experimental values seems to indicate that the multiplicity of the dissociating $InCH_3$ is singlet and that the dissociation of $Ga(CH_3)_2$ produces a triplet $Ga(CH_3)$. Jacko and Price[11] argued that the lower than expected reaction rate constant for the second methyl dissociation of Ga-$(CH_3)_3$ was presumably due to a change in multiplicity from triplet to singlet state as the second methyl radical is released. The present work seems to confirm that $Ga(CH_3)$ is produced as a triplet but that it is a singlet $InCH_3$ the species that dissociates. A calculation for the dissociation of $In(CH_3)_3$ at equilibrium at 1000 K results in only singlet $InCH_3$.

The average ratios between calculated and experimental rate constants for the dissociation reactions of Table 2 and the ratios calculated at average temperatures using Arrhenius parameters for other dissociation reactions shown in Table 3 are depicted as a histogram in Figure 3. Thus, for $In(CH_3)_3$, $In(CH_3)$, Ga-$(CH_3)_3$, and $Ga(CH_3)_2$, we have chosen the information from Table 2, which was obtained at specific temperatures and pressures. For NH_3, PH_3, and AsH_3, we displayed the data from Table 2. In the case of NH_3, we have shown results at 45 and 0.2 atm. The nine reactants are indicated along the abscissa. From left to right, the first five reactions involve dissociation of a methyl radical; the last four involve dissociation of a hydrogen atom. Along the positive ordinate, we show the ratios between calculated and experimental reaction rate constant and, along the negative ordinate, the ratios between experimental and calculated. The worst result corresponds to the dissociation of the $In(CH_3)$ radical, with a calculated value 90 times smaller than the experimental value. The values reported by Buchan and Jasinski[16] for NH_3, PH_3, and AsH_3 at high pressures are actually based on an approximated preexponential factor and

TABLE 3: Ratios between Calculated and Experimental Rate Constants Obtained from Arrhenius Parameters at the Specified Temperature

	log A	E_a/R (K)	avg T (K)	ratio
$In(CH_3)_3 \rightarrow In(CH_3)_2 + CH_3$				
predicted k_{uni}	11.42	17795		
$T = 550-663$ K; $P = 13$ Torr; [toluene]/[In] > 150[13]	15.72	23752	607	1
ref 12 reevaluation	16.10	24154		1
predicted k_∞	20.60	27552		
$^1In(CH_3) \rightarrow {}^2In + CH_3$				
predicted k_{uni}	9.72	21356		
$T = 680-781$ K; $P = 13$ Torr; [toluene]/[In] > 150[13]	10.91	19474	731	1/204
predicted k_∞	17.12	25446		
$Ga(CH_3)_3 \rightarrow Ga(CH_3)_2 + CH_3$				
predicted k_{uni}	9.96	18449		
$T = 686-839$ K; $P = 13$ Torr; [toluene]/[Ga] = 45−120[11]	15.54	29941	763	9
ref 12 reevaluation	16.10	30696		7
ref 17 reevaluation	16.91	32357		9
ref 17 MIDI-1	16.33	31300		9
ref 17 MP3/MIDI-1	17.45	33414		11
ref 2 reevaluation	14.27	27375		6
predicted k_∞	20.32	32314		
$Ga(CH_3)_3 \rightarrow Ga(CH_3)_2 + CH_3$				
predicted k_{uni}	20.61	33111		
$T = 300-600$ K; $P = 22$ Torr; 1% in He[2]	14.20	28432	450	78
predicted k_∞	21.32	33700		
$Ga(CH_3)_2 \rightarrow {}^3Ga(CH_3) + CH_3$				
predicted k_{uni}	10.41	26101		
$T = 829-983$ K; $P = 13$ Torr; [toluene]/[Ga] = 45−120[11]	7.94	17819	906	1/32
predicted k_∞	20.20	36919		
$Al(CH_3)_3 \rightarrow Al(CH_3)_2 + CH_3$				
predicted k_{uni}	8.60	17787		
$T = 850-950$ K; $P = 20$ Torr; 0.5% in argon[16]	16.10	32709	900	1/2
predicted k_∞	19.73	35456		
$AsH_3 \rightarrow AsH_2 + H$				
predicted k_{uni}	14.56	32068		
$T = 850-950$ K; $P = 10^6$ Torr; 0.5% in argon[16]	15.74	37691	900	34
predicted k_∞	18.15	36241		
$PH_3 \rightarrow PH_2 + H$				
predicted k_{uni}	14.55	35644		
$T = 850-950$ K; $P = 10^6$ Torr; 0.5% in argon[16]	15.74	41515	900	44
predicted k_∞	18.28	40063		
$NH_3 \rightarrow NH_2 + H$				
predicted k_{uni}	11.43	36016		
$T = 2200-3300$ K; $P = 45$ atm; 0.3% in argon[16]	15.74	54250	2750	1/27
predicted k_∞	17.82	48955		
$NH_3 \rightarrow NH_2 + H$				
predicted k_{uni}	9.07	36016		
$T = 2200-3300$ K; $P = 0.2$ atm; 0.3% in argon[15]	10.55	47200	2750	2
predicted k_∞	17.82	48955		

estimates for the activation energy based on spectroscopically determined heats of formation. The predicted NH_3 at high pressure (45 atm) was 27 times smaller than the reported value. The second radical of the sample, $Ga(CH_3)_2$, gave a calculated value 16 times smaller than the experimental value. All other comparisons were within a factor of 8, including NH_3 at low pressure (0.2 atm).

The accuracy of the calculations should be compared to the uncertainty in the experimental values. For example, the

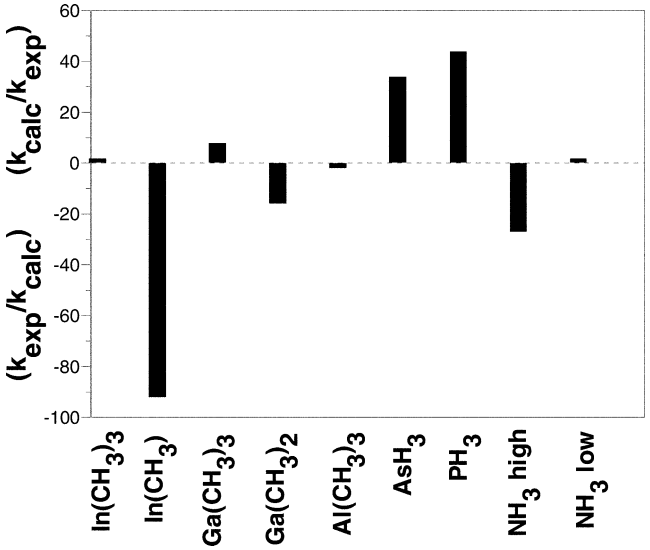

Figure 3. Comparison between calculated and experimental reaction rate constants. From left to right, the first five reactions correspond to the dissociation of one methyl radical and the last four to the dissociation of one hydrogen atom. NH_3 high and low correspond to high- and low-pressure values, respectively.

experimental data by Jacko and Price[11] for the first methyl dissociation of $Ga(CH_3)_3$ at 13 Torr and temperatures between 740 and 840 K may be fit into the following Arrhenius equation:

$$\ln k\,(s^{-1}) = (23.67 \pm 2.40) - \frac{(19\,923 \pm 1892)}{T} \quad (22)$$

When the upper and lower values for the rate constants are calculated at the average temperature of 763 K, one obtains rate constants that are about 130 times larger and smaller than the base value. With the use of *t*-distribution values for a 95% confidence interval on ln k and for 29 degrees of freedom, the prediction interval for the rate constant at 763 K results in values that are 3.7 times larger and smaller than the base value. Our predicted value (see Table 3) is 9 times larger than the corresponding experimental value.

The data for $In(CH_3)_3$ by Jacko & Price[13] can be fit into the following equation, including the standard errors:

$$\ln k\,(s^{-1}) = (36.14 \pm 1.02) - \frac{23\,650 \pm 625}{T} \quad (23)$$

The lowest and highest values calculated from eq 23 at 607 K are about 8 times lower and higher than the base value. With the use of *t*-distribution values for a 95% confidence interval on ln k and for 18 degrees of freedom, the prediction interval for the rate constant at 607 K results in values that are 1.7 times larger and smaller than the base value. Our predicted value (see Table 3) is about the same as the experimental value.

As described under Method, the simulation of the simple model for the dissociation of $In(CH_3)_3$ in an OMVPE reactor (eqs 9−15) required (a) the thermodynamic parameters for each species, specified according to eqs 17−19, (b) the Lennard-Jones and Sutherland parameters for calculating transport properties, and (c) the Arrhenius parameters for the forward and reverse reaction rate constants for eqs 9−15. Table 4 contains the parameters used for the transport properties of the indium species.

Standard third-law entropies for ethane and hydrogen gas, calculated based on our coefficients (see eqs 17 and 19), gave

TABLE 4: Estimated Intermolecular Parameters for the Indium Species

	6-12 Lennard-Jones		Sutherland			
molecule	ϵ/k_B (K)	σ (Å)	ϵ/k_B (K)	σ (Å)	A (kg/(s m K$^{1/2}$))	B (K)
$In(CH_3)_3$	433	5.20	439	6.53	8.045×10^{-7}	76.12
$In(CH_3)_2$	393	5.08	397	6.39	8.019×10^{-7}	68.99
$In(CH_3)$	352	4.94	355	6.21	8.024×10^{-7}	61.70
In	309	4.79	312	6.03	8.021×10^{-7}	54.08

TABLE 5: Standard Heat of Formation (H_f°/R)[a]

species	exptl values
In (g)	29 287[43]
$In(CH_3)$ (g)	19 575[43]
$In(CH_3)_3$ (g)	20 682[43]
H_2 (g)	0
CH_3 (g)	16 706[43]
C_2H_6 (g)	−10 192[44]

Heat of Formation for $In(CH_3)_2$ $P = 1$ atm

	reaction 1 $In(CH_3)_3 \rightarrow In(CH_3)_2 + (CH_3)$	reaction 2 $In(CH_3) + CH_3 \rightarrow In(CH_3)_2$	avg
calculated $\Delta H_{reac}/R$	30 020	−12 929	
heat of formation	28 158	23 352	25 755

[a] Units of K.

excellent agreement with experimental data: the calculated values for S°_{3-law}/R were 27.4 and 15.7 for ethane and hydrogen gas, respectively, and the corresponding experimental values were 27.6 and 15.7. Consequently, the z_7 used in these calculations were those obtained directly by fitting the calculated data. The z_6 coefficients (see eq 16) were obtained from experimental standard heats of formation plus the z_1-z_5 coefficients obtained by fitting the calculated data (see eq 18). The experimental values of heat of formation used for the indium atom, $In(CH_3)$, $In(CH_3)_3$, and the methyl radical are taken from Clark and Price;[43] the value for $In(CH_3)_2$ is obtained from a quantum mechanical calculated heat of reaction plus experimental heats of formation of all other species for the following reactions:

$$In(CH_3)_3 \rightarrow In(CH_3)_2 + CH_3 \quad (24)$$

$$In(CH_3) + CH_3 \rightarrow In(CH_3)_2 \quad (25)$$

Table 5 contains the experimental and calculated heats of formation, divided by the gas constant, for all species of the simplified model. The complete set of parameters used for the thermodynamic properties is contained in Table 6. We have also included in Table 6 the complete set of calculated Arrhenius parameters for all reactions considered.

A statistical thermodynamic calculation of the equilibrium concentration of all the species at 300 and 1000 K and 1 and 20 atm showed that from a thermodynamical point of view most of the indium would be present as singlet $In(CH_3)$ even at 300 K. At 1000 K, there would also be free In (about 15%). Please refer to Table 7. A similar analysis on $Al(CH_3)_3$ and $Ga(CH_3)_3$ resulted in a fully undissociated $Al(CH_3)_3$ at 300 K, 0.1% $Al(CH_3)$ at 1000 K, 0.4% $Ga(CH_3)$ at 300 K, and 17% $Ga(CH_3)$ at 1000 K. There is experimental evidence that $In(CH_3)_3$ does not dissociate at 300 K. These results seem to indicate that the aluminum and gallium compounds do not dissociate at 300 K because of thermodynamic reasons, whereas the indium compound does not dissociate because of the kinetics of its dissociation.

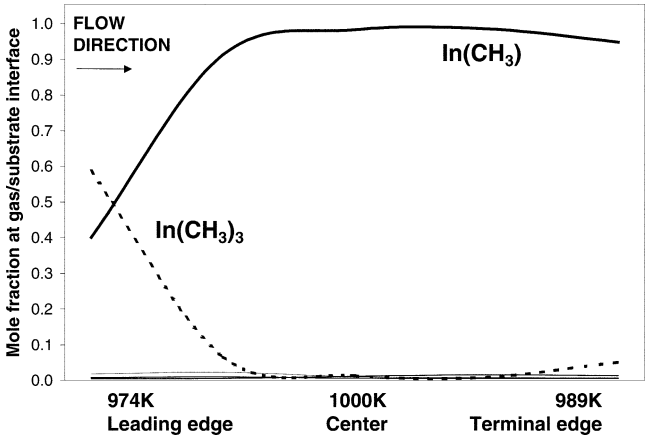

Figure 4. Mole fractions at the gas/substrate interface from the decomposition of $In(CH_3)_3$ in a compact hard-shell reactor at 1 atm. The boundary wall at the substrate was set to 1000 K and all other walls to 300 K. The abscissa displays the position of the substrate and the temperature at the gas/substrate interface.

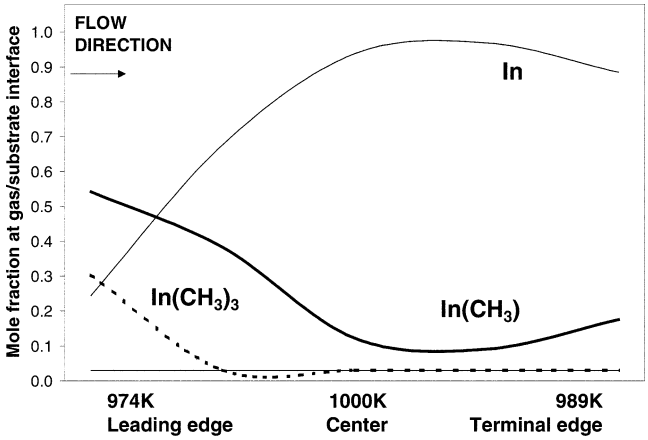

Figure 5. Mole fractions at the gas/substrate interface from the decomposition of $In(CH_3)_3$ in a compact hard-shell reactor at 20 atm. The boundary wall at the substrate was set to 1000 K and all other walls to 300 K. The abscissa displays the position of the substrate and the temperature at the gas/substrate interface.

To confirm this hypothesis, a purely chemical kinetic model was solved by finite differences for the forward and reverse eqs 9, 10, and 12, and the reverse eq 15. The calculations were performed at 300 and 1000 K and at 1 and 20 atm. At 300 K, using a time increment of 1×10^{-4} s and after 4 h, no detectable $In(CH_3)_3$ dissociation occurred. At 1000 K, using a time increment of 1×10^{-12} s and after 0.1 s, the mole fractions were 0.284 and 0.280 for $In(CH_3)_3$ at 1 and 20 atm, respectively, 0.003 for $In(CH_3)_2$, 0.462 for $In(CH_3)$, and 0.251 and 0.255 for In at 1 and 20 atm, respectively.

As stated under Method, the fluid dynamic simulations for the dissociation of trimethylindium were performed at 1 and 20 atm. The carrier gas was N_2 at a flow rate of 12 standard liters per minute, and the mass fraction for $In(CH_3)_3$ was 2×10^{-4}. The reactor consisted of a grid of 90 657 cells and 109 570 nodes, the concentration of grid cells being larger in the region of the substrate. The inlet temperature was 300 K, and the temperature of the walls at the substrates was 1000 K.

We discuss first the resulting steady-state concentrations along the midpoint between the upper and lower substrates (or centerline of the reactor). At the leading edge of the substrates, 98% and 96% of the $In(CH_3)_3$ is undissociated at 1 and 20 atm, respectively. Moving along the centerline toward the terminal edge of the substrate, the concentration of $In(CH_3)_3$ decreases

TABLE 6: Predicted Coefficients for the Thermodynamic and Chemical Kinetic Properties

Coefficients for Thermodynamic Properties[a]

species	z_1	z_2	z_3	z_4	z_5	z_6	z_7
			$P = 1$ atm				
In	2.50	4.62×10^{-14}	-9.02×10^{-17}	6.10×10^{-20}	-1.65×10^{-23}	28 541	6.64
$InCH_3s$	3.02	1.29×10^{-2}	-9.20×10^{-6}	3.82×10^{-9}	-6.72×10^{-13}	18 135	9.02
$InCH_3t$	2.95	1.30×10^{-2}	-9.27×10^{-6}	3.76×10^{-9}	-6.41×10^{-13}	18 135	9.02
$In(CH_3)_2$	3.22	2.67×10^{-2}	-1.85×10^{-5}	7.22×10^{-9}	-1.20×10^{-12}	23 386	8.75
$In(CH_3)_3$	3.73	4.02×10^{-2}	-2.67×10^{-5}	9.94×10^{-9}	-1.58×10^{-12}	17 474	5.46
CH_3	3.77	2.90×10^{-3}	1.61×10^{-6}	-1.57×10^{-9}	3.33×10^{-13}	15 438	2.64
C_2H_6	3.62	4.00×10^{-3}	1.90×10^{-5}	-1.60×10^{-8}	3.71×10^{-12}	−11 604	5.62
			$P = 20$ atm				
In	2.50	1.60×10^{-13}	-2.84×10^{-16}	1.80×10^{-19}	-3.97×10^{-23}	28 541	3.65
$InCH_3s$	3.49	1.07×10^{-2}	-6.05×10^{-6}	1.93×10^{-9}	-2.77×10^{-13}	18 135	3.09
$InCH_3t$	3.09	1.24×10^{-2}	-8.46×10^{-6}	3.29×10^{-9}	-5.45×10^{-13}	18 135	3.09
$In(CH_3)_2$	3.73	2.46×10^{-2}	-1.54×10^{-5}	5.44×10^{-9}	-8.34×10^{-13}	23 386	0.78
$In(CH_3)_3$	4.40	3.76×10^{-2}	-2.30×10^{-5}	7.83×10^{-9}	-1.16×10^{-12}	17 474	−7.15
CH_3	3.68	3.38×10^{-3}	8.04×10^{-7}	-1.05×10^{-9}	2.19×10^{-13}	15 438	−3.23
C_2H_6	2.54	9.56×10^{-3}	1.01×10^{-5}	-1.03×10^{-8}	2.47×10^{-12}	−11 604	−0.99

Coefficients for Kinetic Properties[b] for $T = 700-1000$ K

	$P = 1$ atm		$P = 20$ atm	
reaction	ln A	E_a/R	ln A	E_a/R
$In(CH_3)_3 \rightarrow In(CH_3)_2 + CH_3$	36.92	23 661	41.69	25 450
$In(CH_3)_2 + CH_3 \rightarrow In(CH_3)_3$	22.10	−5 739	29.85	−3 949
$In(CH_3)_2 \rightarrow In(CH_3)s + CH_3$	19.64	6 616	22.63	6 616
$In(CH_3)s + CH_3 \rightarrow In(CH_3)_2$	12.26	−5 498	18.25	−5 497
$In(CH_3)_2 \rightarrow In(CH_3)t + CH_3$	32.27	29 418	35.26	29 418
$In(CH_3)t + CH_3 \rightarrow In(CH_3)_2$	23.72	−5 585	29.71	−5 584
$In(CH_3)s \rightarrow In + CH_3$	32.18	26 462	35.16	26 458
$In + CH_3 \rightarrow In(CH_3)s$	25.96	9 748	31.94	9 746
$In(CH_3)t \rightarrow In + CH_3$	17.20	1 220	20.20	1 220
$In + CH_3 \rightarrow In(CH_3)t$	12.16	7 395	18.14	7 396
$C_2H_6 \rightarrow 2CH_3$	33.48	38 419	36.48	38 419
$2CH_3 \rightarrow C_2H_6$	16.06	−4 834	22.04	−4 833

Equilibrium Constants for $In(CH_3)s \leftrightarrow In(CH_3)t$[c]

T (K)	$P = 1$ atm	$P = 20$ atm
700	1.77×10^{-14}	5.72×10^{-14}
800	1.07×10^{-12}	3.43×10^{-12}
900	2.60×10^{-11}	8.29×10^{-11}
1000	3.34×10^{-10}	1.06×10^{-9}

[a] Refer to eqs 17−21. [b] Refer to eq 16. [c] Refer to eq 14.

TABLE 7: Equilibrium Concentrations for the Dissociation of $In(CH_3)_3$ Assuming Model Eqs 9−15

	$P = 1$ atm		$P = 20$ atm	
species	$T = 300$ K	$T = 1000$ K	$T = 300$ K	$T = 1000$ K
In doublet	3.31×10^{-7}	0.138	4.35×10^{-7}	0.155
$In(CH_3)$ singlet	1.000	0.862	1.000	0.845
$In(CH_3)$ triplet	1.73×10^{-33}	2.88×10^{-10}	6.14×10^{-33}	8.95×10^{-10}
$In(CH_3)_2$ doublet	1.66×10^{-16}	4.22×10^{-8}	1.06×10^{-15}	2.64×10^{-7}
$In(CH_3)_3$ singlet	3.09×10^{-11}	2.03×10^{-10}	2.89×10^{-10}	1.96×10^{-9}
CH_3 doublet	6.84×10^{-28}	6.77×10^{-6}	1.92×10^{-28}	1.81×10^{-6}
C_2H_6 singlet	1.000	1.069	1.000	1.077
sum on indium	1.000	1.000	1.000	1.000
sum on carbon	3.000	3.000	3.000	3.000

to 56% and 35% at 1 and 20 atm, respectively. At 1 atm, the main dissociation product is singlet $In(CH_3)$, followed by free In. At 20 atm, there is as much $In(CH_3)$ as free In.

We proceed to consider the steady-state concentrations at the gas/substrate interface. Figures 4 and 5 show the molar fractions of the four indium species [$In(CH_3)_3$, $In(CH_3)_2$, $In(CH_3)$, and In] at pressures of 1 and 20 atm, respectively. The abscissa displays the location of the substrate for a flow direction from left to right and the temperatures at the gas/substrate interface in contact with the leading edge, center, and ending of the substrates. From the dotted lines, at the leading edge of the substrates there is about 60% and 35% undissociated $In(CH_3)_3$ at 1 and 20 atm, respectively. When we move along the substrates in the direction of the flow, a dramatic difference occurs between the two figures regarding the dissociation products: at 1 atm, most indium is present as singlet $In(CH_3)$, whereas at 20 atm, most is present as free In.

If, for practical reasons, the temperature of the substrate needs to be reduced in OMVPE, a way of increasing $In(CH_3)_3$ dissociation would be to reduce the flow rate. But, to maintain laminar flow, a condition that is required for homogeneous epitaxy, the Grashof number (Gr) must be much smaller than the square of the Reynolds number (Re), as defined by eqs 26 and 27.

$$Gr = \frac{h^2 \mathbf{g} \rho^2 \beta_T \Delta T}{\mu^2} \tag{26}$$

$$Re = \frac{\rho u h}{A P \mu} \tag{27}$$

where h is the channel height, $\mathbf{g}$ the gravity vector, ρ the density of the fluid, β_T the volume coefficient of expansion, ΔT the change in temperature in the channel, μ the viscosity of the gas, u the standard flow rate, A the cross-sectional area, and P

the standard pressure. From eqs 26 and 27, it can be seen that the Ge/Re^2 ratio is proportional to $\mathbf{g}(P/u)^2$. Therefore, on the ground, high-pressure OMVPE must be carried out at a sufficiently high flow velocity to maintain a small Ge/Re^2 ratio. Alternatively, under conditions of reduced gravity, an increase in P could be coupled with a smaller u without an onset of turbulence.

Conclusions

Calculations of the reaction rate constants for the homolytic dissociation of group III and group V were performed on the basis of quantum mechanical calculations and transition-state theory. The critical configuration was determined using linear interpolation to determine the structures, Morse's potential for the electronic energy, and Hase's relationship for the vibrational frequencies. The Troe approach was used for calculating the bimolecular component, k_{bim}, of the unimolecular rate constant, k_{uni}.

Comparison of predicted reaction rate constants with experimentally determined values showed that the predicted reaction rate constants for $In(CH_3)_3$, $Ga(CH_3)_3$, $Al(CH_3)_3$, and low-pressure NH_3 are within 8 times the experimental values. This uncertainty compares very well with the uncertainty in the experimental data. Calculated rate constants for the dissociation of the $Ga(CH_3)_2$ and $In(CH_3)$ radicals were 16 and 92 times smaller than experimental values, respectively. Our predicted values for high-pressure AsH_3 and PH_3 were 34 and 44 times larger than the estimated values reported by Buchan and Jasinski,[16] and that for high-pressure NH_3 was 27 times smaller. The present computations of reaction rate constants seem to confirm that $Ga(CH_3)$ is produced as a triplet, and they seem to indicate that the dissociating monomethylindium species is a singlet state.

Finally, we performed a fluid dynamic simulation for the dissociation of trimethylindium in a compact hard-shell reactor based on a simplified set of chemical reactions. The simulations were solved at a substrate temperature of 1000 K, at a flow rate of 12 slm, and at 1 and 20 atm of pressure. Increasing the pressure from 1 to 20 atm resulted in an increase of $In(CH_3)_3$ dissociation. The main dissociation product at the gas/substrate interface at 1 atm was $In(CH_3)$ and at 20 atm was free In. The main dissociation product at the centerline between the substrates at 1 atm was $In(CH_3)$, and at 20 atm, there were equal amounts of $In(CH_3)$ and free In.

Acknowledgment. The investigation reported in this paper has been possible through the partial support provided by the NASA Alliance for Nonlinear Optics (Grant NAG8-1708, subcontract from New Mexico Highlands University) and NASA Cooperative Agreement NCC8-194. One of the authors (B.H.C.) acknowledges the NASA Summer Faculty Fellowship Program at Marshall Space Flight Center, where many of the ideas of the research discussed in this paper were generated.

References and Notes

(1) Ambacher, O.; Brandt, M. S.; Dimitrov, R.; Metzger, T.; Stutzmann, M.; Fischer, R. A.; Miehr, A.; Bergmaier, A.; Dollinger; G. *J. Vac. Sci. Technol., B* **1996**, *14*, 3532.

(2) Larsen, C. A.; Buchan, N. I.; Li, S. H.; Stringfellow, G. B. *J. Cryst. Growth* **1990**, *102*, 103.

(3) Cardelino, B. H.; Moore, C. E.; Cardelino, C. A.; Frazier, D. O.; Bachmann, K. J. *J. Phys. Chem. A* **2001**, *105*, 849.

(4) Marcus, R. A. *J. Chem. Phys*. **1952**, *20*, 359.

(5) Troe, J. *J. Chem. Phys*. **1977**, *66*, 4750.

(6) Troe, J. *J. Chem. Phys*. **1977**, *66*, 4758.

(7) Troe, J. *J. Phys. Chem*. **1979**, *83*, 114.

(8) Bamford, C. H., Tipper, C. F. H., Eds. *Comprehensive Chemical Kinetics*; Elsevier: Amsterdam, 1972; Vol. 4.

(9) Suzuki, N.; Anayama, C.; Masu, K.; Tsubouchi, K.; Mikoshiba, N. *Jpn. J. Appl. Phys.* **1986**, *25*, 1236.

(10) Squire, D. W.; Dulcey, C. S.; Lin, M. C. *Chem. Phys. Lett*. **1985**, *116*, 525.

(11) Jacko, M. G.; Price, S. J. W. *Can. J. Chem.* **1963**, *41*, 1560.

(12) Smith, G. P.; Patrick, R. *Int. J. Chem. Kinet.* **1983**, *15*, 167.

(13) Jacko, M. G.; Price, S. J. W. *Can. J. Chem*. **1964**, *42*, 1198.

(14) Buchan, N. I.; Larsen, C. A.; Stringfellow, G. B. *J. Cryst. Growth* **1988**, *92*, 605.

(15) Holzrichter, K.; Wagner, H. Gg. 18th International Symposium on Combustion, Combustion Institute, Pittsburgh, 1981. In *Combustion Chemistry*; Gardiner, W. C., Jr., Ed.; Springer-Verlag: New York, 1984; pp 384−385.

(16) Buchan, N. I.; Jasinski, J. M. *J. Cryst. Growth* **1990**, *106*, 227.

(17) Oikawa, S.; Tsuda, M.; Morishita, M.; Mashita, M.; Kuniya, Y. *J. Cryst. Growth* **1988**, *91*, 471.

(18) Su, J. Z.; Teitelbaum, H. *Int. J. Chem. Kinet.* **1994**, *26*, 159.

(19) Robinson, P. J.; Holbrook, J. A. *Unimolecular Reactions*; Wiley-Interscience: London, 1972.

(20) Gardiner, W. C., Jr.; Troe, J. In *Combustion Chemistry*; Gardiner, W. C., Jr., Ed.; Springer: New York, 1984.

(21) Lindemann, F. A. *Trans. Faraday Soc*. **1922**, *17*, 598.

(22) Kajimoto, O. In *The Transition State; A Theoretical Approach*; Fueno, T., Ed.; Gordon and Breach Science Publishers: Tokyo, 1999; Chapter 5.

(23) Quack, M.; Troe, J. *Ber. Bunsen-Ges. Phys. Chem.* **1974**, *78*, 240.

(24) Truhlar, D. G. *J. Chem. Phys*. **1970**, *53*, 2041.

(25) Truhlar, D. G.; Garrett, B. C. *Acc. Chem. Res.* **1980**, *13*, 440.

(26) Wardlaw, D. M.; Marcus, R. A. *Chem. Phys. Lett*. **1984**, *110*, 230.

(27) Wardlaw, D. M.; Marcus, R. A. *J. Phys. Chem.* **1986**, *90*, 5383.

(28) Fulle, D.; Hippler, H.; Striebel, F. *J. Chem. Phys*. **1998**, *108*, 6709.

(29) Hippler, H.; Siefke, M.; Stark, H.; Troe, J. *Phys. Chem. Chem. Phys*. **1999**, *1*, 57.

(30) Hippler, H.; Otto, B.; Schroeder, J.; Schubert, V.; Troe, J. *Ber. Bunsen-Ges. Phys. Chem.* **1985**, *89*, 240.

(31) Hippler, H.; Luther, K.; Ravishankara, A. R.; Troe, J. *Z. Phys. Chem. Neue Folge* **1985**, *142*, 1.

(32) Lucas, K. *Applied Statistical Thermodynamics*; Springer-Verlag: Berlin, Heidelberg, 1991.

(33) Becke, A. D. *J. Chem. Phys*. **1996**, *104*, 1040.

(34) Adamo, C.; Barone, V. *Chem. Phys. Lett*. **1997**, *274*, 242.

(35) Hohenberg, P.; Kohn, W. *Phys. Rev.* **1964**, *B136*, 864.

(36) Kohn, W.; Sham, L. J. *Phys. Rev.* **1965**, *A150*, 1133.

(37) Parr, R. G.; Yang, W. *Density-functional theory of atoms and molecules*; Oxford University Press: Oxford, U.K., 1989.

(38) Frisch, M. J.; Trucks, G. W.; Schlegel, H. B.; Scuseria, G. E.; Robb, M. A.; Cheeseman, J. R.; Zakrzewski, V. G.; Montgomery, J. A., Jr.; Stratmann, R. E.; Burant, J. C.; Dapprich, S.; Millam, J. M.; Daniels, A. D.; Kudin, K. N.; Strain, M. C.; Farkas, O.; Tomasi, J.; Barone, V.; Cossi, M.; Cammi, R.; Mennucci, B.; Pomelli, C.; Adamo, C.; Clifford, S.; Ochterski, J.; Petersson, G. A.; Ayala, P. Y.; Cui, Q.; Morokuma, K.; Malick, D. K.; Rabuck, A. D.; Raghavachari, K.; Foresman, J. B.; Cioslowski, J.; Ortiz, J. V.; Stefanov, B. B.; Liu, G.; Liashenko, A.; Piskorz, P.; Komaromi, I.; Gomperts, R.; Martin, R. L.; Fox, D. J.; Keith, T.; Al-Laham, M. A.; Peng, C. Y.; Nanayakkara, A.; Gonzalez, C.; Challacombe, M.; Gill, P. M. W.; Johnson, B. G.; Chen, W.; Wong, M. W.; Andres, J. L.; Head-Gordon, M.; Replogle, E. S.; Pople, J. A. *Gaussian 98*, revision A.7; Gaussian, Inc.: Pittsburgh, PA, 1998.

(39) Hase, W. L. *J. Chem. Phys*. **1972**, *57*, 730.

(40) *CFD-ACE*; CFD Research Corporation: Huntsville, AL, 1998.

(41) Byrd, R. B.; Stewart, W. E.; Lightfoot, E. N. *Transport Phenomena*; John Wiley & Sons: New York, 1960.

(42) Berkowitz, J.; Ellison, G. B.; Gutman, D. *J. Phys. Chem.* **1994**, *98*, 2744.

(43) Clark, W. D.; Price, S. J. W. *Can. J. Chem.* **1968**, *46*, 1633.

(44) *Lange's Handbook of Chemistry*, 11th ed.; Dean, J. A., Ed.; McGraw-Hill Book Co.: New York, 1973.